JOURNAL OF SOLID STATE CHEMISTRY 65, 100–110 (1986)

A Study of the Ternary Oxide $LiVO_2$ and Its Anomalous Behavior

T. A. HEWSTON* AND B. L. CHAMBERLAND

Department of Chemistry and Institute of Materials Science, University of Connecticut, Storrs, Connecticut 06268

Received November 4, 1985; in revised form March 10, 1986

Nonstoichiometric $LiVO_2$ and its unusual magnetic, electrical, and thermal phase transition near 200°C were studied using X-ray diffraction, IR and EPR spectroscopy, thermoanalytical methods, and measurements of electrical resistivity and magnetic susceptibility. The transition is semireversible, appearing to be noncooperative and of higher or multiple order. It has been concluded that the driving force for the transition is not a structural instability, but rather a critical distance phenomenon involving a change in the V^{3+}–V^{3+} bond type. The low-temperature data are interpreted in terms of a two-dimensional vanadium "metal cluster layer" formed via covalent-type metal-to-metal bonds; above T_t, narrow-band metallic behavior sets in within the vanadium planes. The phase transition in $LiVO_2$ is similar to that of $TiCl_3$, and is also very similar to the semiconducting-to-metallic transformations in VO_2 and V_2O_3.

Introduction

The preparation of the compound $LiVO_2$ was first reported in 1954 by Rüdorff and Becker (*1*). The compound was obtained as a black powder, and X-ray diffraction indicated a trigonal structure isotypic with that of α-$NaFeO_2$. This structure is a sodium chloride derivative in which the different cations are segregated on alternate (111) cubic planes. It is depicted in Figs. 1a and b from a "cubic" and a "hexagonal" point of view, respectively.

Magnetic effects indicating the existence of a phase transition in $LiVO_2$ were first reported in 1957 by Bongers (*2*). A fourfold increase in the molar magnetic susceptibility was observed upon heating through 450 K; at higher temperatures the susceptibility displayed only slight temperature dependence.

Reuter *et al.* (*3*) reported an abrupt decrease in electrical resistivity as $LiVO_2$ was heated through 180°C; semiconducting behavior was observed in the polycrystalline sample both above and below the transition temperature.

Kobayashi and co-workers (*4*) conducted a detailed study of the $Li_xV_{2-x}O_2$ system using high-temperature X-ray powder diffraction and measurements of specific heats, magnetic susceptibilities, and electrical resistivities. The earlier results of Bongers and Reuter for $LiVO_2$ were confirmed, and the endothermic (upon heating) transition enthalpy was measured. The transition was characterized by reversibility and hysteresis. The high-temperature X-

* Present address: Chemistry Division (Code 3854), Research Dept., Naval Weapons Center, China Lake, CA 93555.

0022-4596/86 $3.00

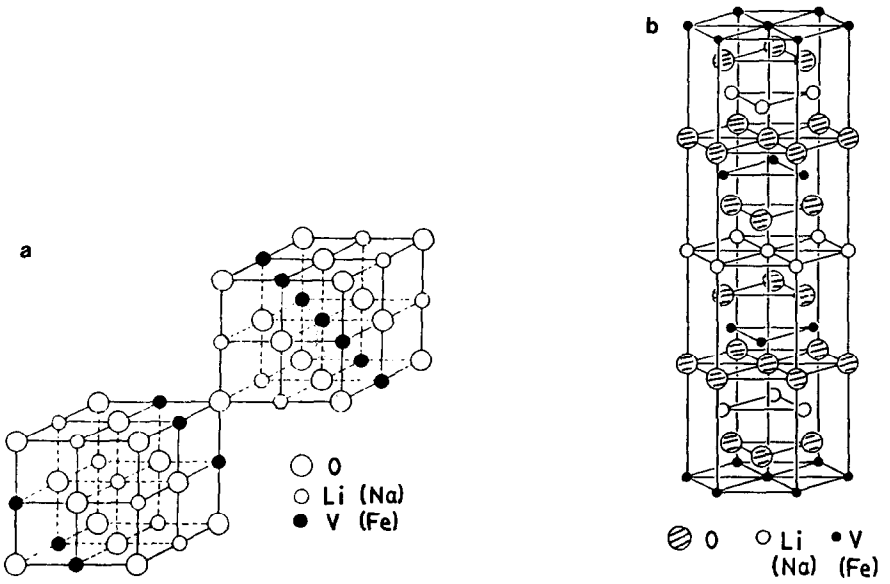

FIG. 1. The α-$NaFeO_2$ structure ($R\bar{3}m$): (a) "cubic" point of view; (b) "hexagonal" point of view.

ray diffraction results indicated a discontinuous volume change at the transition temperature, T_t, but no change in symmetry was observed. Upon heating through T_t the hexagonal a axis was found to expand whereas the c axis contracted, resulting in an overall volume increase of 1–2%.

A mechanism for the phase transition involving complex antiferromagnetism in a two-dimensional triangular array was proposed by Bongers (*2*). Goodenough (*5*) and Kobayashi (*4*) have suggested the formation of triangular vanadium metal clusters in the low-temperature region (*6*). Since no crystallographic distortion could be detected by X-ray powder diffraction below T_t and single crystals were unavailable for detailed structural studies, experimental support for these suggested mechanisms has been lacking.

Typical preparations of $LiVO_2$ powder have employed reactions between lithium carbonate and vanadium oxides. Evidence for the formation of $LiVO_2$ via the electrochemical reduction of $LiVO_3$ in a LiCl–KCl eutectic has also been reported (*7*). A second polymorph of $LiVO_2$ has been obtained in the form of black cubic crystals using high-pressure methods (*8*). A single-crystal X-ray diffraction study indicated a cubic atacamite-type sodium chloride superstructure. Recently, the preparation of crystals of α-$NaFeO_2$-type $LiVO_2$ has been reported (*9*). The crystals exhibited two morphologies—hexagonal platelets and octahedral dendrites—and were obtained using a fused-salt electrolytic method. The Gandolfi X-ray diffraction patterns of the crystals were very similar, while TGA and EPR results indicated similar, nonstoichiometric compositions.

The present report describes the results of an in-depth study of the $LiVO_2$ system, which was found to be nonstoichiometric. The nature of the unusual phase transition has been investigated, and a semiconducting-to-metallic mechanism is proposed.

Experimental Methods

Polycrystalline Li_xVO_2 was prepared by reacting lithium carbonate with V_2O_5 under

a flowing argon/hydrogen mixture (10 : 1, respectively). Stoichiometric quantities of the reactants plus a 5% excess of Li_2CO_3 were thoroughly ground together in an agate mortar and then heated in an alumina boat in two steps. The first heating of a typical 3 to 5-g preparation was carried out at 625°C for 14 hr. Samples were cooled abruptly just outside the heating zone under the reducing atmosphere, reground, and reheated at 750°C for 4 hr. Subsequent heating did not detectably alter X-ray diffraction patterns or stoichiometry. Excess lithium carbonate could be removed from the product by leaching with dilute acetic acid. X-ray powder diffraction indicated no sample degradation by this treatment. Crystals of Li_xVO_2 were obtained in the form of brilliant black hexagonal platelets and octahedral-like dendrites using a fused-salt electrolytic method described elsewhere (*9*).

Experimental methods employed for chemical analysis, X-ray diffraction, thermogravimetric analysis (TGA), differential scanning calorimetry (DSC), and measurement of magnetic susceptibilities have been previously described (*9*). A high-temperature X-ray camera (Central Research Laboratories, Inc.) was used to obtain the powder patterns of polycrystalline samples above and below the transition temperature. Crude resistivity measurements were made on compressed (25 tons) disks (8 mm diam; 0.1 mm thick) of Li_xVO_2 powder and dendritic crystals. Resistance was measured directly with a Keithley 177 μV DMM multimeter using an *x-y* recorder and a chromel-alumel thermocouple; the sample pellet was heated in a silica tube in a tube-type furnace under flowing nitrogen. Infrared spectra of finely ground powders in KBr pellets were obtained in the 4000- to 400-cm^{-1} region with a Nicolet Model 60SX FTIR spectrophotometer. A high-temperature pellet transmission cell (Barnes Co.) with a temperature controller was used to obtain spectra at various temperatures. X-band EPR spectra of neat powder samples at 80 and 298 K were obtained using a Varian E-3 spectrometer.

Results

As described previously (*9*), atomic absorption spectrophotometry and TGA have indicated that $LiVO_2$ powder and both types of $LiVO_2$ crystals are similarly lithium-deficient. The TGA results indicate a common formula of $Li_{0.7}VO_2$.[1] This implies the presence of 0.3 mole V^{4+} per mole of compound. The presence of a substantial quantity of an odd-electron species was supported by the observation of a strong, although uncalibrated, EPR signal from $Li_{0.7}VO_2$ powder at 80 K.

The anomalous magnetic behavior accompanying the phase transitions in the various forms of $Li_{0.7}VO_2$ is shown in Fig. 2. In general, heating through the phase transition is accompanied by a marked increase in susceptibility. In the high-temperature region, the temperature dependence of the susceptibility is greatly reduced. Slight differences in magnetic behavior are observed for the various forms of $Li_{0.7}VO_2$; the magnetic transition is weakest in the platelet-type crystals. All the samples, however, exhibit unique first-cycle curves with higher transition temperatures and greater hysteresis than in subsequent heatings; this unique first-cycle behavior did not reappear in a sample which was allowed to rest for months after 17 DSC cycles. In all of the freshly prepared samples, the observed magnetic moments were lowest prior to the first heating through the transition temperature. An irreversible component of the phase transition apparently causes a permanent increase in magnetic

[1] In the TGA analyses under flowing oxygen (*9*), each mole of Li_xVO_2 takes up $[(1 + x)/4]$ moles O_2 upon complete oxidation.

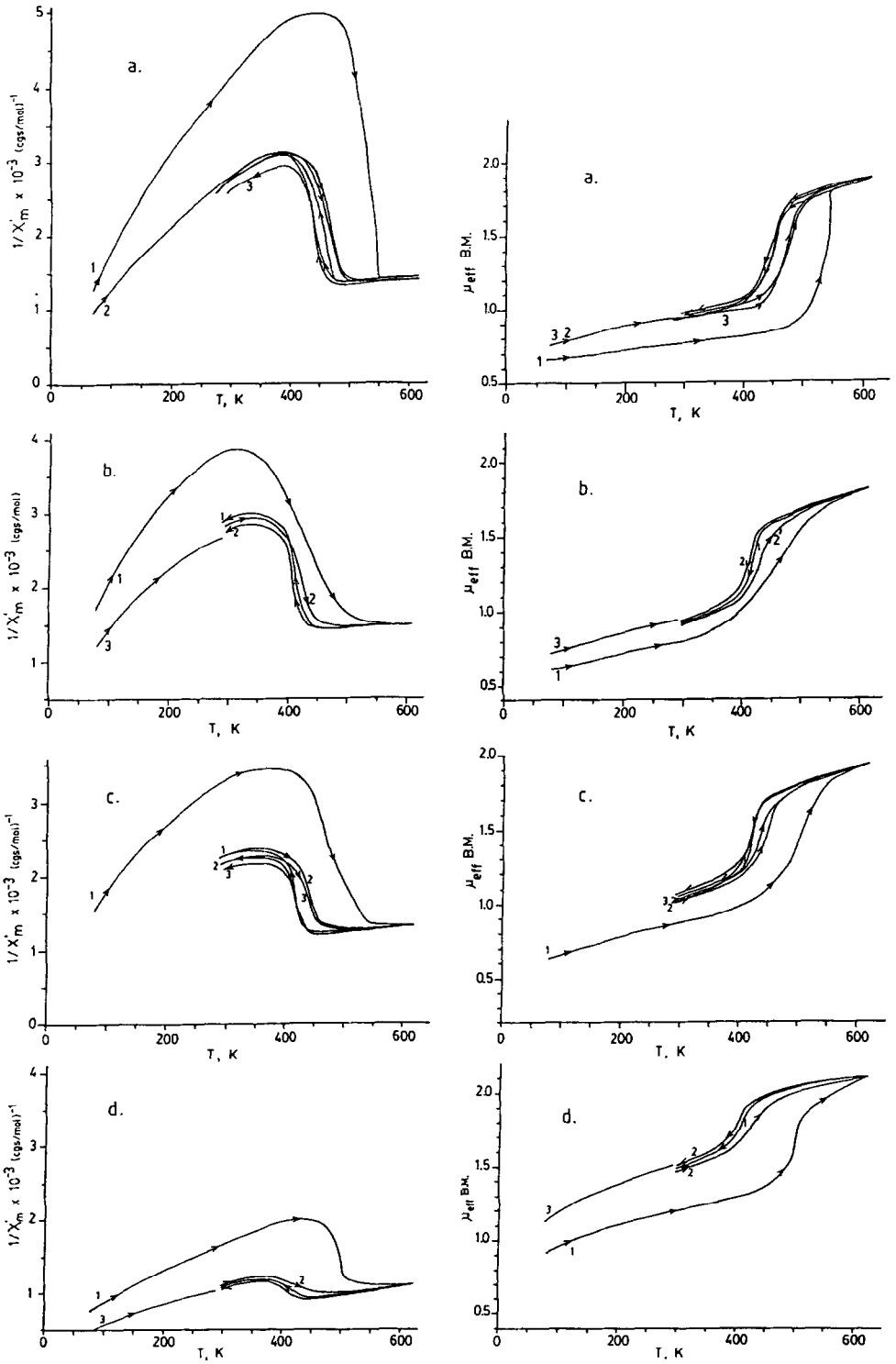

FIG. 2. Magnetic behavior of various forms of $Li_{0.7}VO_2$—inverse susceptibility and effective moment vs temperature: (a) powder; (b) dendrites (well crystallized); (c) dendrites (poorly crystallized); (d) platelets.

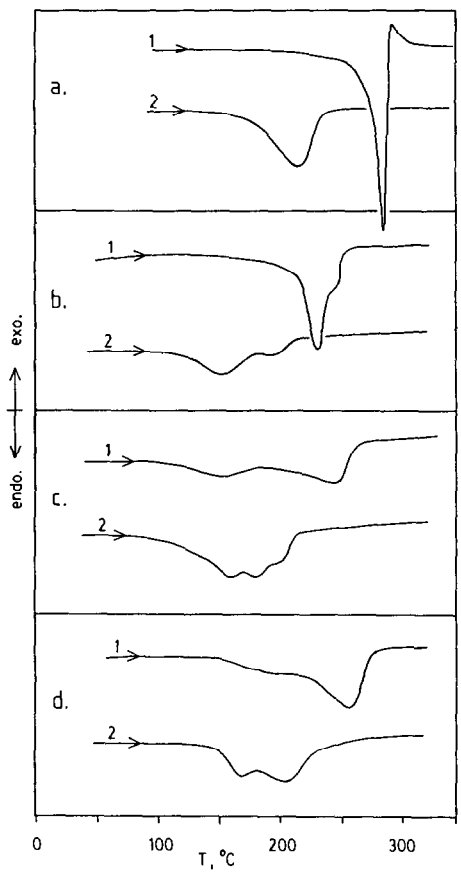

FIG. 3. First- and second-cycle endotherms for $Li_{0.7}VO_2$: (a) powder; (b) platelets; (c) dendrites, well crystallized; (d) dendrites, poorly crystallized.

moment and decrease in transition temperature.

Similar semireversibility and dependence upon sample history is observed in the thermal effects which accompany the phase transition. The DSC curves of two heating cycles for the various forms of $Li_{0.7}VO_2$ are given in Fig. 3; X-ray diffraction patterns of samples before and after cycling were unchanged. Differences in the shapes of the curves, transition temperatures, and associated enthalpies are observed. The endothermic enthalpies for the various forms varied from 500 to 1000 cal/mole. This quantity of heat is similar to that associated with the phase transition near 70°C in VO_2 (800 cal/mole) which has been associated with a crystallographic distortion and the formation of V^{4+}–V^{4+} pairs.

As seen in Figs. 2 and 3, the phase transition in $Li_{0.7}VO_2$ is very gradual and takes place over a 50 to 100° temperature range. The transition mechanism appears to be strongly affected by kinetic factors and is very sensitive to heating rate. As seen in Fig. 4, the phase transition is almost nondetectable by DSC when the heating rate is decreased by an order of magnitude. This is consistent with a gradual, as opposed to cooperative (*10*), mechanism. Although the volume discontinuity and observation of hysteresis might be interpreted as first-order character, the gradual, noncooperative nature of the phase transition in $Li_{0.7}VO_2$ indicates that a multiple- or higher-order process is occurring. The transition is also characterized by a strong dependence on sample history; surface energy, particle size, and grain boundaries may have important thermodynamic effects.

The electrical/ionic conductivity effects accompanying the phase transition in $Li_{0.7}VO_2$ are shown in Fig. 5. Since polycrystalline samples were used, only a qualitative statement can be made: as $Li_{0.7}VO_2$ is heated through its phase transition, a substantial increase in conductivity occurs.

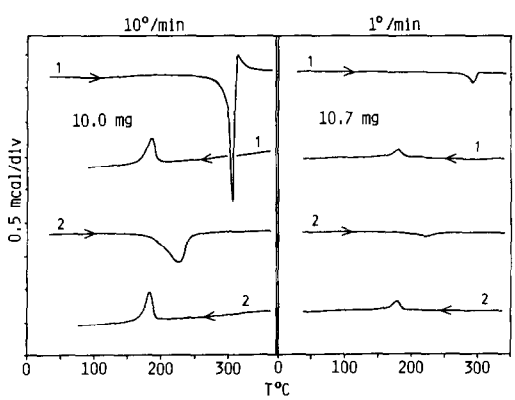

FIG. 4. DSC of $Li_{0.7}VO_2$ powder at different heating rates.

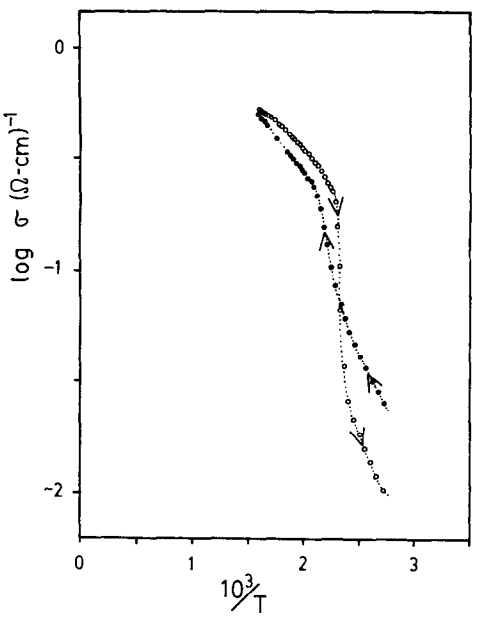

FIG. 5. Conductivity vs reciprocal temperature (K) of a compressed disk of $Li_{0.7}VO_2$ dendrites.

Infrared spectra of $Li_{0.7}VO_2$ powder at various temperatures during the heating and cooling portions of a first heating cycle are shown in Fig. 6. The absorption band near 870 cm^{-1} is due to a trace of Li_2CO_3 which was not removed from this sample. As seen in Fig. 6a, the infrared spectrum of $Li_{0.7}VO_2$ above the phase transition becomes very broad, and the prominent bands at 715 and 605 cm^{-1} are virtually absent. These bands reappear as the compound is cooled through T_t, as seen in Fig. 6b. These observations are consistent with covalency in the low-temperature region and metallic character above T_t.

Refined unit cell dimensions for various $Li_{0.7}VO_2$ samples are collected in Table I. The Gandolfi patterns of the crystals and the Debye-Scherrer pattern of the powder were nearly identical, with only slight differences in intensities (*9*). The very similar specific volumes, in conjunction with the results of the TGA analyses (*9*), are consistent with a common stoichiometry. As compared with an equivalent-volume hexagonal cell with ideal cubic close packing (ccp) (Table I), it is seen that the room-temperature unit cell of $Li_{0.7}VO_2$ is expanded in the *c* direction and contracted in the *a* direction. This results in an abnormally high *c*/*a* ratio and an unusually small rhombohedral angle (α). Viewed in terms of perfect sphere-packing, the structure is contracted within the cp layers, and expanded in the perpendicular direction. The unit cell data in Table I for $Li_{0.7}VO_2$ powder below and above the transition temperature indicate that as the compound is heated through T_t, this packing distortion relaxes—the *c* axis decreases while the *a* axis increases—and the various parameters approach the ideal ccp values. A 5% volume increase accompanies this process, and no change in symmetry could be detected.

The Gandolfi X-ray powder pattern for the hexagonal platelet-type $Li_{0.7}VO_2$ crystals could be indexed (as indicated in Table I) on the basis of an α-$NaFeO_2$ type hexagonal cell (space group $R\bar{3}m$); however, precession photographs taken of a crystal using long exposure times indicated a hexagonal superstructure with an *a* axis larger by a factor of $2\sqrt{3}$ (*9*).

Precession photographs of a large octahedral-type crystal were anomalous in appearance (*9*). A photograph of the "*hk*0" net, assuming cubic symmetry, is shown in Fig. 7. Symmetrical and selective doubling of certain reflections was consistently observed from sample to sample and could

TABLE I

UNIT CELL PARAMETERS FOR $LiVO_2$ COMPOUNDS

Sample	*a* (Å)	*c* (Å)	*c*/*a*	α°	Å³/*Z*
Powder	2.841(1)	14.75(1)	5.192	31.81	34.37
Dendrites	2.842(1)	14.73(1)	5.183	31.86	34.34
Platelets	2.842(1)	14.75(1)	5.190	31.80	34.39
(Ideal ccp)	*2.897*	*14.19*	*4.90*	*33.57*	*34.40*
Powder, 25°C	2.846	14.87	5.225	31.62	34.77
Powder, 300°C	2.930	14.78	5.044	32.67	36.63

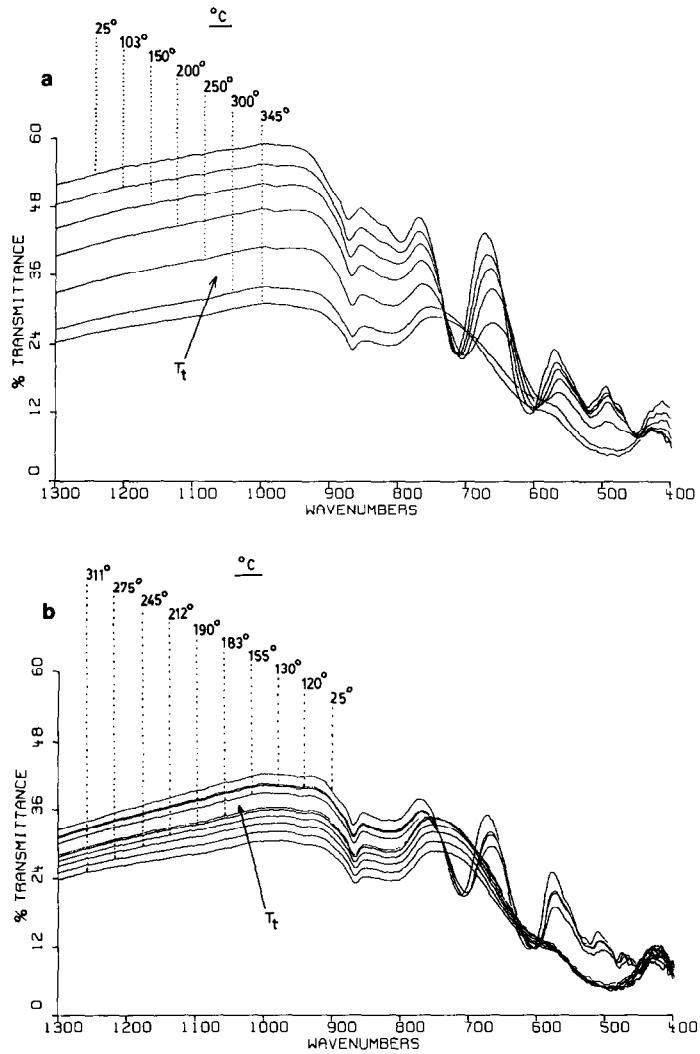

FIG 6. IR spectra of $Li_{0.7}VO_2$ powder during a first heating cycle: (a) heating; (b) cooling.

not be eliminated by improved sample alignment. Calculated X-ray diffraction patterns for $LiVO_2$, $LiVO_2$ with "ideal ccp" cell parameters, and an observed pattern for $Li_{0.7}VO_2$ are given in Figs. 8a–c, respectively. The strongest set of resolved doublets near the center of the precession photograph in Fig. 7 corresponds to the (018) and (110) reflections, seen as moderately strong lines at 31.6 and 32.9° in Figs. 8a,c. Removal of the packing distortion described previously leads to the coalescence of these reflections, as seen in the calculated pattern for $LiVO_2$ with ideal ccp (Table I), shown in Fig. 8b. Similarly, the other doublets observed in the precession photograph correspond to reflection-pairs such as (009)/(107), (00,12)/(024), and (11,12)/(214) which are also observed to coalesce to a single reflection upon idealization of the packing. Although the dendrite-type crystals have adopted a pseudo-cubic habit, the

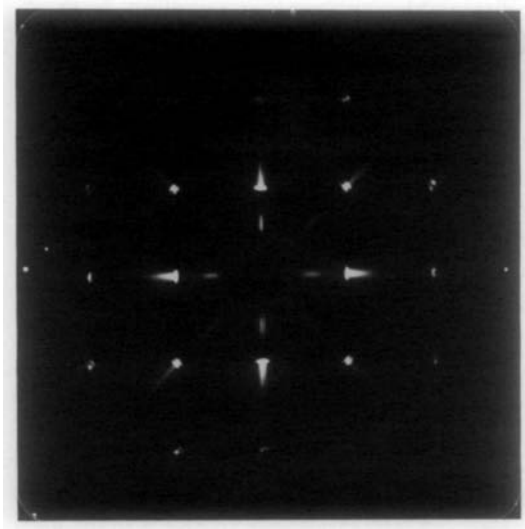

FIG. 7. "*hk*0" net (cubic basis) for octahedral-type $Li_{0.7}VO_2$ crystal.

spot-doublings indicate that the actual symmetry is lower.

Discussion

In the layered NaCl-derived structure of $LiVO_2$, each VO_6 octahedron shares six edges with other VO_6 octahedra within the basal plane. Goodenough has pointed out that in such edge-sharing systems, the strongest interactions may be direct cation-to-cation processes involving no anion intermediary (*5, 10, 11*). The strength of these interactions depends on the cation–cation separation (R) and the occupancy of the d orbitals, especially the t_{2g} set which can be directed toward all the edges of the octahedral coordination polyhedron. The cation–cation interactions are classified as "strong" or "weak," depending on a "critical" intercation separation (R_c), below which direct overlap of the t_{2g} orbitals occurs and the interacting electrons are best described by a collective-electron, Hartree-Fock-type model. When the intercation separation is greater than the critical distance, a localized, Heitler-London-type model is appropriate. Compounds with $R < R_c$ are predicted to be metallic while those with $R > R_c$ should be insulators or semiconductors. When $R \cong R_c$, narrowband metallic behavior is possible as well as semiconductor-to-metallic transformations involving spin pairing in cation–cation bond formation.

In $LiVO_2$, $R = 2.84$ Å $< R_c = 2.94$ Å (*11*). We suggest that the phase transition is driven by a change in the V^{3+}–V^{3+} bond type which results in a semiconducting-to-metallic transformation *within the vanadium planes*. Since the vanadium planes are separated by intervening layers of oxygen, lithium, and oxygen ions, strong interplanar interactions are not likely. The phase transition is therefore a two-dimensional process. The vanadium atoms within a basal plane in the α-$NaFeO_2$ structure are symmetrically equivalent and comprise a hex-

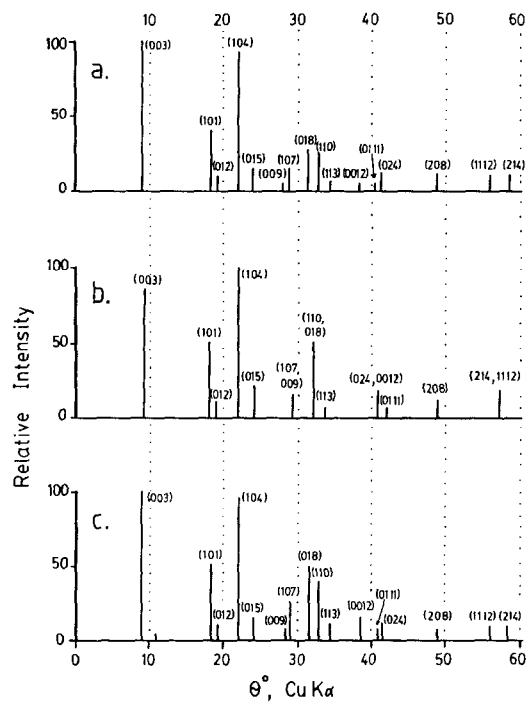

FIG. 8. Calculated X-ray diffraction patterns for (a) $LiVO_2$, $R\bar{3}m$; (b) $LiVO_2$, $R\bar{3}m$, "ideal ccp." Observed X-ray diffraction pattern for (c) $Li_{0.7}VO_2$ dendrites.

agonal, six-connected net. Each vanadium atom is surrounded by six other equidistant and coplanar vanadium atoms at distances indicative of direct t_{2g}–t_{2g} orbital overlap. In the low-temperature region, continuous overlapping of the t_{2g} orbitals throughout the basal plane could facilitate delocalized covalent V^{3+}–V^{3+} bonding, each vanadium plane thus comprising an infinite, hexagonally symmetric, "two-dimensional metal cluster." The average vanadium–vanadium bond in stoichiometric $LiVO_2$ (d^2) would be "$\frac{1}{3}$" of a single V^{3+}–V^{3+} covalent bond. This bonding scheme in the low-temperature region is consistent with the packing distortion observed in the $LiVO_2$ system—contraction within the layers and elongation perpendicular to them. Above the transition temperature, this packing distortion relaxes as the compound becomes a two-dimensional narrow-band metal. In this model, no change in lattice symmetry is required since the vanadium bonding is axially symmetric in both the high- and low-temperature phases. This is in agreement with crystallographic studies which have thus far detected no such symmetry change. The absence of a symmetry lowering is also consistent with the observed noncooperative, gradual nature of the phase transition (*10*). Since lithium ions do not appear to be directly involved in the phase transition, and since the critical distance for V^{4+} is predicted to be the same as that for V^{3+} (*11*), the process occurring in $Li_{0.7}VO_2$ may not be fundamentally different from that occurring in the stoichiometric compound.

The relatively low magnetic susceptibility, the nature of the infrared spectra, and the reduced conductivity observed in the low-temperature region are consistent with covalent bonding in $Li_{0.7}VO_2$ below T_t. In addition, Bongers and Locher (*6, 12*) have obtained ^{51}V NMR spectra of $LiVO_2$ at various temperatures; below T_t the spectrum was temperature independent and exhibited appreciable quadrupolar coupling, both effects being consistent with covalency. This spectrum is remarkably similar to that of VO_2 (*13*) in its low-temperature region with covalently bonded V^{4+}–V^{4+} pairs.

The ^{51}V NMR results (*6, 12*) also provide evidence of metallic behavior in $LiVO_2$ above the phase transition: upon heating through T_t, the intensity of the signal abruptly decreased and was reduced to a single resonance with no observable quadrupolar interaction. These observations are consistent with itinerant electrons and metallic-like bonding above T_t. The chemical shift was temperature-independent and slightly larger in the high-temperature region—an effect similar to the Knight shift observed in metallic systems—and its magnitude (+0.61%) was nearly the same as that observed for vanadium metal (+0.58%) (*14*).

The relatively featureless infrared spectra of $Li_{0.7}VO_2$ above T_t obtained in the present study also indicate metallic bonding in the high-temperature phase. Although enhanced conductivity is observed in this region, experimental confirmation to date of an increasing resistivity with temperature above T_t may have been precluded by the use of polycrystalline samples and the two-dimensional nature of the metallic interaction. Anisotropic electrical resistivity measurements on large single crystals of $LiVO_2$ are needed. However, narrow-band metallic behavior in the high-temperature region is indicated by the minimal temperature dependence of the magnetic susceptibility, which has been measured up to 1150 K by Bongers (*6, 12*). This behavior is nearly identical to that of VO_2 and V_2O_3 (*5*), which are known to undergo semiconductor-to-metal transformations; furthermore, the magnitude of the susceptibility observed for $Li_{0.7}VO_2$ above T_t is intermediate between those of VO_2 and V_2O_3 in their high-temperature, metallic regions. As in the $LiVO_2$ system, the corundum-type

structure of V_2O_3 exhibits an anomalously large c/a value, which has been similarly attributed to metal–metal interactions across shared octahedral edges (*15*).

The transition in $Li_{0.7}VO_2$ is strikingly similar to that of $TiCl_3$ (*16, 17*). $TiCl_3$ adopts the two-dimensional $FeCl_3$ structure; Ti^{3+} (d^1) ions occupy two-thirds of the octahedral sites in alternate layers of a close-packed chloride matrix. The positions of the metals within the layers form a hexagonal three-connected net, which is derived from the six-connected vanadium net in $LiVO_2$ by removing one-third of the metal ions. Compared to V^{3+} (d^2) in $LiVO_2$, each Ti^{3+} has half as many Ti^{3+} neighbors as well as half as many d electrons; the coplanar cation–cation interactions across shared octahedral edges are expected to be strong because of the short titanium–titanium distance (*5*). The magnetic profile of the phase transition in $TiCl_3$ near 200 K (*16*) is very similar to that of $LiVO_2$, but the temperature dependence of the magnetic susceptibility above T_t as well as anisotropic electrical resistivity measurements on single crystals (*17*) indicate that the high-temperature region is characterized by localized rather than itinerant electron behavior. The transition in $TiCl_3$ is therefore of the semiconductor-to-semiconductor type. As in the $LiVO_2$ system, discontinuities in the hexagonal a and c axes were observed, but no change in symmetry was detectable; the formation of a "bonding-band" within the titanium layers below T_t was suggested (*16*).

Conclusion

The thermal and magnetic properties of the semireversible phase transition in $Li_{0.7}VO_2$ were studied in detail. The first heating cycles of all forms (crystals and powder) consistently displayed unique properties and were always accompanied by the largest hysteresis effects. The transition is very gradual in nature and appears to be noncooperative and of higher or multiple order. The details of the properties are markedly dependent upon sample form and history. By considering all the available experimental data, it has been concluded that the driving force for the transformation is not a structural instability, but rather a critical distance phenomenon involving a change in the V^{3+}–V^{3+} bond type from covalent to metallic. An interpretation of the process has been offered and is based on the formation, in the low-temperature region, of a two-dimensional "metal cluster layer" via covalent-type V^{3+}–V^{3+} bonds. Above the transition temperature, $LiVO_2$ becomes a two-dimensional narrow-band metal. Similarities have been pointed out between the transition in the $LiVO_2$ system and the semiconductor-to-semiconductor transition in $TiCl_3$, and the semiconductor-to-metal transitions in VO_2 and V_2O_3. The layered α-$NaFeO_2$ structure of $LiVO_2$ permits the formation of a comprehensive electronic network linking all the coplanar transition metal ions via a continuous overlapping of t_{2g} orbitals. This appears to be an optimal structural arrangement for permitting strong, direct cation–cation interactions which seem to typify other interesting vanadium-oxygen systems such as V_2O_3, V_4O_7, and VO_2.

Acknowledgment

The authors extend thanks to Dr. Melvin P. Nadler of NWC for obtaining the IR spectra.

References

1. W. RÜDORFF AND H. BECKER, *Z. Naturforsch. B* **9**, 613, 614 (1954).
2. P. F. BONGERS, Ph.D. Dissertation, The University of Leiden, Leiden, The Netherlands, 1957.
3. B. REUTER, R. WEBER, AND J. JASKOWSKI, *Z. Elektrochem.* **66**, 832 (1962).
4. K. KOBAYASHI, K. KOSUGE, AND S. KACHI, *Mat. Res. Bull.* **4**, 95 (1969).

5. J. B. GOODENOUGH, "Magnetism and the Chemical Bond," Interscience, New York, 1963.
6. P. F. BONGERS, *in* "Crystal Structure and Chemical Bonding in Inorganic Chemistry" (C. J. M. Rooymans and A. Rabenau, Eds.), Chap. 4, North-Holland, Amsterdam, 1975.
7. R. B. CHESSMORE AND H. A. LAITINEN, *J. Electrochem. Soc.* **122,** 238 (1975).
8. C. CHIEH, B. L. CHAMBERLAND, AND A. F. WELLS, *Acta Crystallogr. Sect. B* **37,** 1813 (1981).
9. T. A. HEWSTON AND B. L. CHAMBERLAND, *J. Solid State Chem.* **59,** 168 (1985).
10. J. B. GOODENOUGH, *Phys. Rev.* **117,** 1442 (1960).
11. J. B. GOODENOUGH, *in* "Progress in Solid State Chemistry," Vol. 5, Chap. 4 (H. Reiss, Ed.), Pergamon, New York, 1971.
12. P. F. BONGERS AND P. R. LOCHER, personal communication, 1983.
13. K. NARITA, J. UMEDA, AND H. KUSUMOTO, *J. Chem. Phys.* **44,** 2719 (1966).
14. L. E. DRAIN, *Proc. Phys. Soc.* **83,** 755 (1964).
15. C. T. PREWITT, R. D. SHANNON, D. B. ROGERS, AND A. W. SLEIGHT, *Inorg. Chem.* **8,** 1985 (1969).
16. S. OGAWA, *J. Phys. Soc. Jpn.* **15,** 1901 (1960).
17. F. CAVALLONE, I. POLLINI, AND G. SPINOLO, *Lett. Nuovo Cimento* **4,** 764 (1970).